Research Article

Received: 14 June 2017 Revised: 25 August 2017 Accepted article published: 4 September 2017 Published online in Wiley Online Library:

(wileyonlinelibrary.com) DOI 10.1002/jctb.5428

Titanium dioxide-coated biochar composites as adsorptive and photocatalytic degradation materials for the removal of aqueous organic pollutants

Xiaoxi Cai,[a,b,c] Jiang Li,[a,b*] Yunguo Liu,[a,b*] Zhili Yan,[a,b] Xiaofei Tan,[a,b] Shaobo Liu,[d,e] Guangming Zeng,[a,b] Yanling Gu,[a,b] Xinjiang Hu[f] and Luhua Jiang[a,b]

Abstract

BACKGROUND: This article reports the synthesis and characterisation of titanium dioxide-coated biochar composites (TBCs) by pyrolysing titanium dioxide-treated biomass prepared by a modified sol–gel method. Their adsorptive and photocatalytic activities were evaluated based on the removal of safranine T (ST) from an aqueous solution with/without UV-light irradiation.

RESULTS: Characterisation studies suggested that TiO_2 was successfully loaded on the biochar substrate. The biochar and TiO_2 contents of the composite significantly affected its performance. The ST removal capabilities of the TBCs with 1, 1.5, 2, and 2.5 g of the biomass are 1.7, 2.3, 7.2, and 2.3 times better than that of the raw biochar, respectively. Thus, the optimum amount of biomass in TBC-x was determined to be 2 g, with the corresponding sample exhibiting excellent stability, effectiveness over a wide pH range, and a maximum ST removal capacity of 226.7 mg g^{-1}.

CONCLUSION: The loading of TiO_2 significantly enhanced the adsorption performance of biochar and the high specific surface area of the biochar synergistically promoted the photocatalytic activity of TiO_2. Both adsorption and photocatalytic degradation were confirmed to contribute to the decolourisation of the aqueous solution because of the removal of ST, with the effect of adsorption being slightly higher than that of photocatalysis. The synthesised composite is a promising alternative material for removing chemical contaminants.

Keywords: biochar; titanium dioxide; composite; adsorption; photocatalytic; degradation

ABBREVIATIONS

TBC-x	Titanium dioxide-coated biochar composite (TBC-x)
BC	Biochar (BC)
ST	Safranine T (ST)
SEM	Scanning electron microscopy (SEM)
FTIR	Fourier transform infrared spectroscopy (FTIR)
XRD	X-ray diffraction (XRD)
XPS	X-ray photoelectron spectroscopy (XPS).

INTRODUCTION

Biochar (BC) is a carbonaceous product of the pyrolysis of biomass. It exhibits some desirable properties such as a large surface area, good ion exchange capacity, and high porosity, and has abundant oxygen functional groups and an aromatic surface.[1,2] Recently, there have been various reports on the utilisation of BC for wastewater treatment and remediation of contaminated soil, owing to its cost-effectiveness for the removal of chemical contaminants, namely, heavy metals and organic contaminants.[3–8] There have also been several interesting proposals for the use of BC as a

* *Correspondence to: J Li or Y Liu, College of Environmental Science and Engineering, Hunan University, Changsha 410082, P.R. China. E-mail: lijiang@hnu.edu.cn (Li); hnuliuyunguo@gmail.com (Liu)*

a *College of Environmental Science and Engineering, Hunan University, Changsha, P.R. China*

b *Key Laboratory of Environmental Biology and Pollution Control, Hunan University, Changsha, P.R. China*

c *College of Art and Design, Hunan First Normal University, Changsha, P.R. China*

d *School of Architecture and Art, Central South University, Changsha, P.R. China*

e *School of Metallurgy and Environment, Central South University, Changsha, P.R. China*

f *College of Environmental Science and Engineering, Central South University of Forestry and Technology, Changsha, P.R. China*

stabiliser of nano-sized metal oxides which tend to aggregate because of their high surface energy and strong magnetic attraction, leading to reduced effective surface area and contact area when used for the removal of pollutants.[9–14] For instance, Jung *et al.* explored combined electrochemical modifications for the fabrication of a MgO/biochar composite which exhibited excellent aqueous phosphate adsorption properties represented by a Langmuir–Freundlich maximum adsorption capacity of 620 mg-P g^{-1}.[15] Zhang *et al.* synthesised a magnetic BC material through thermal pyrolysis and demonstrated that the material is an excellent sorbent for the removal of arsenic (V) from an aqueous solution. The magnetic BC exhibited an adsorption capacity of 3147 mg kg^{-1} toward As(V) and an excellent ferromagnetic property that is favourable for the separation of the sorbent from the solution.[16] Wang *et al.* prepared manganese oxide-modified BC via precipitation and found that modification of BC with birnessite provided an effective means of producing low-cost carbon sorbents for the removal of heavy metals.[17] All these previous studies demonstrate the feasibility of producing nanocomposite adsorbents based on BCs, with nano-sized metal oxides attached to their surfaces. This strategy is expected to gain popularity because it not only enhances the stability of the nano-sized metal oxides, but also retains the properties of both the BC and metal oxide components.[1,2]

Photocatalysis based on TiO_2 is particularly attractive because of its wide availability, low cost, and non-toxicity.[18–21] Recently, TiO_2 and its composites have been extensively utilised as photocatalysts for the removal of dyes from wastewater.[22] For example, Zhang *et al.* demonstrated a UV–visible light photocatalysis process for the degradation of azo dyes using TiO_2.[23] Vinu and Madras considered a combination of sono- and photo-catalytic degradation of anionic dyes with TiO_2 synthesised by a solution combustion process (and commercial TiO_2). They found that the rates of the simultaneous sono-photocatalytic degradation of all the considered dyes and the reduction of the total organic carbon species were higher compared with those corresponding to separate photocatalytic and sonocatalytic processes.[24] Wang *et al.* developed effective piezoelectric semiconductor-based hybrid photocatalysts by assembling TiO_2 nanoparticles on ZnO monocrystalline nanoplatelets. These photocatalysts could be used as heterojunction band structures to achieve significant photocatalytic performance enhancement in a wide range of applications, owing to improved charge separation.[25] Thus, a composite of TiO_2 and porous BC could exhibit excellent performance for the removal of dyes through both adsorption and photocatalytic processes. However, few attempts have been made to examine the adsorption and photocatalytic properties of such composites.

The primary objective of this study was to fabricate TiO_2-coated biochar (TBC) by pyrolysing TiO_2-treated biomass prepared by a modified sol–gel method. The as-fabricated composites were characterised by scanning electron microscopy (SEM), Fourier transform infrared spectroscopy (FTIR), X-ray diffraction (XRD), and X-ray photoelectron spectroscopy (XPS). The adsorption and photocatalytic degradation of safranine T (ST) in the presence of the fabricated TiO_2-coated biochar were investigated under different conditions through batch experiments. Factors controlling their activity, such as the material dosage, pH, initial ST concentration, and contact time were examined in detail. Based on the findings, possible mechanisms of ST removal by TiO_2-coated biochar are proposed.

EXPERIMENTAL MATERIALS AND METHODS

Materials

Titanium butoxide ($Ti(OC_4H_9)_4$, 98%) was used as the TiO_2 precursor, ramie bar was used as the biomass, and glacial acetic acid (CH_3COOH, 99.8%) and ethanol (C_2H_5OH, 99.7%) were used as the catalyst and solvent, respectively. The target test sample ST (>98.5% pure) was purchased from Sinopharm Chemical Reagent Co., Ltd. All the other reagents were obtained from local chemical suppliers and used without further purification. Ultrapure water generated by a Millipore Milli-Q water purification system was used for all the experiments.

Synthesis of TiO_2-coated biochar composites

Raw BC used for the synthesis was obtained as described elsewhere.[26–28] The ramie bars used as the biomass were obtained from farms in Changsha City, Hunan Province, China. After air-drying at room temperature, the biomass was ground and sieved through a 100 mesh sieve (0.149 mm). Then, it was pyrolysed at 500 °C under a nitrogen flow at 50 mL min^{-1} in a muffle furnace with a tubular reactor, for 2 h. The heating rate of the furnace was set to 5 °C min^{-1}. The BC obtained was cooled and washed at least three times with ultrapure water. This was followed by drying at 80 °C for 24 h, and subsequent sieving to a particle size of 0.149 mm.

The TBC-x composites were prepared following a previously reported modified sol–gel method.[29] The precursor alkoxide solution consisted of 10 mL of titanium butoxide completely dissolved in 15 mL of ethanol. After vigorous stirring for 40 min at room temperature, different amounts of the powdered biomass (1, 1.5, 2, and 2.5 g) were added to the titanium butoxide solutions in ethanol. Then, 15 mL of a solution of 1:1:1 glacial acetic acid, ethanol, and water was added dropwise to each of the mixtures under magnetic stirring, using a burette. The resulting mixtures were stirred at room temperature until a turmeric-coloured sol was formed. Each sol sample was aged in air at 40 °C for 2 h, followed by gelation and subsequent drying of the gel at 80 °C for 24 h. The dried gel was subsequently ground into a fine powder and calcined at 500 °C in a flow of N_2 for 2 h, to yield TBC-x. The different TBC-x samples are referred as TBC-1, TBC-1.5, TBC-2, and TBC-2.5, respectively, based on the amount of added biomass.

Characterisation methods

The surface morphologies and structures of raw BC and the synthesised composite catalysts were characterised by SEM (JEOL JSM-6700, Japan). The specific surface area of raw BC and composite catalysts was estimated via nitrogen adsorption measurements (at 77.3 K) performed using a Micromeritics TriStar II 3020 instrument. The structural properties of the composite catalysts were characterised using a D/max-rB XRD system (Rigaku D/max-2500, Japan) with Cu $K\alpha$ radiation ($\lambda = 1.541$ Å) at 40 kV and 30 mA over the 2θ range 10–90°. The FTIR spectra of the materials were recorded on a spectrophotometer (Nicolet 6700 spectrometer, USA) over the wave number range 400–4000 cm^{-1} at room temperature. The chemical states of the elements near the surface of the composite catalysts were examined using an ESCALAB 250 Xi X-ray photoelectron spectrometer (Thermo Fisher, USA).

Experimental procedure

The capacity of TBC-x to remove contaminants from a solution was evaluated based on the decomposition of ST in an aqueous

solution, under UV irradiation. In each experiment, 0.4 g of the TBC-x sample was added to 200 mL of an aqueous ST solution to obtain a suspension. An 8-W UV lamp emitting 365-nm light was placed over the suspension to illuminate it. Before UV irradiation, the aqueous ST solution was stirred in the dark for 1 h to achieve adsorption/desorption equilibrium with the substrate. The ST removal experiment was also performed in a reactor using raw BC.

At pre-set reaction intervals, 5 mL of the suspension was retrieved from the reaction mixture and centrifuged immediately at 4000 rpm for 10 min. The ST content in the supernatant was determined based on the absorbance at 530 nm, using a calibration curve. All the experiments were performed at room temperature under weakly alkaline pH conditions of the ST solution (pH ~8.0), except when the effect of pH was investigated. During the experiments, the reaction mixture was continuously stirred using a magnetic stirrer.

The amount of the degraded ST was calculated using the following formula[30]:

$$qe = \frac{(C0\text{-}Ce)\,V}{m} \quad (1)$$

where C_0 and C_e are the initial and equilibrium ST concentrations (mg L^{-1}), respectively; V is the volume of the ST solution (L); and m is the mass of the composite (g).

The removal of ST was monitored by retrieving 5 mL aliquots of the reactants at pre-set time intervals. The amount of ST removed at these intervals was calculated using the following equation[31]:

$$qt = \frac{(C0\text{-}Ct)\,V}{m} \quad (2)$$

where q_t is the amount of ST removed (mg g^{-1}); C_t is the concentration of the ST solution at time t; V is the volume of the ST solution (L); and m is the mass of the composite (g).

RESULTS AND DISCUSSION

Characterisation of the composites

All the characterisation is discussed for TBC-2 nanocomposite chosen as a representative sample. Representative SEM micrographs of TBC-2 are shown in Fig. 1(a) and (b). As shown, some small TiO_2 particles are attached to the surface of the BC substrate. This confirms the successful loading of TiO_2 particles on the BC surface. The specific surface area and total pore volume of raw BC are 3.29 $m^2\ g^{-1}$ and 0.007 $cm^3\ g^{-1}$, which increased to 10.55 $m^2\ g^{-1}$ and 0.019 $cm^3\ g^{-1}$, respectively, for the TBC-2 nanocomposite. Figure 1(c) shows the XRD pattern of TBC-2, in which, several TiO_2 peaks are clearly observed. Specifically, 10 peaks are observed at 2θ values of 25.32°, 37.85°, 48.05°, 53.89°, 54.97°, 62.85°, 68.85°, 70.21°, 75.04°, and 82.8°. These peaks are consistent with the standard XRD data of the anatase phase TiO_2 diffraction peaks corresponding to the (1 0 1), (0 0 4), (2 0 0), (1 0 5), (2 1 1), (2 0 4), (1 1 6), (2 2 0), (2 1 5), and (2 2 4) planes, respectively.[32] This indicates the successful synthesis of TiO_2 in the form of crystalline anatase in TBC-2. No peaks corresponding to the rutile phase ($2\theta = 27.48°$) are observed, indicating the formation of only the anatase phase (JCPDS card no. 21-1272) during synthesis of the supported catalysts.

Based on the XRD results, the crystal size of the microspheres was determined using Scherrer's formula[33]:

$$L = \frac{K\lambda}{\beta \cos`} \quad (3)$$

where L is the crystal size (nm); λ is the wavelength of the X-ray radiation (0.15418 nm); K is typically 0.89; and β is the line width at the half-maximum height after correcting for the equipment broadening for the peak at $2\theta = 25.32°$. The crystal size of the microspheres was determined to be 27.53 (nm).

The FTIR spectra of BC and TBC-2 are shown in Fig. 1(d). The strongest absorption peak observed at 3430 cm^{-1} is attributed to O-H stretching,[34] whereas the peak at 1621–1629 cm^{-1} could be attributed to the stretching vibrations of O–H or that of ketonic C=O.[35,36] The bands at 2925 and 2854 cm^{-1} are assigned to the stretching vibrations of C–H,[37] whereas that at 1399 cm^{-1} is either due to the bending vibrations of C–H in methyl groups or the bending vibrations of O–H in carboxylic acids. The peak at 1121 cm^{-1} in the IR spectra of TBC-2 corresponds to the Ti-O stretching vibrations,[38] indicating that TiO_2 is coated on the BC surface with the aid of oxygen functionalities. Moreover, the addition of TiO_2 produced a peak within 1010–1300 cm^{-1}, attributed to the C–O stretching band of ether. The FTIR spectra thus indicate the presence of increased amounts of oxygen functional groups such as C=O, C–O, and O=C–O in the TBC-x catalyst, after carbonisation.

The characteristic peaks corresponding to the main elements are observed in the XPS spectra of TBC-2 shown in Fig. 2. The Ti 2p peak is clearly observed, confirming the presence of TiO_2 in the synthesised material. The spectra also indicate that the TBC sample contains O, C, and N, with the peaks reflecting the respective contents of the surface elements. Interestingly, the loaded TiO_2 had an O:Ti ratio of more than 2:1, which might be attributed to the presence of O on the BC surface.

As shown in Fig. 2, the Ti 2p core level spectrum contains two main peaks corresponding with Ti 2p3/2 and Ti 2p1/2. The spectrum indicates that the oxidation state of titanium is primarily Ti^{4+}, with a small amount of Ti^{3+}. Figure 2(b) shows the normalised Ti 2p core level XPS spectra of TBC-2. The two broad peaks centred at 464.7 and 459.1 eV correspond to the characteristic Ti 2p1/2 and Ti 2p3/2 peaks of Ti^{4+}.[39,40] An extra peak observed at 458.58 eV is consistent with the characteristic Ti 2p3/2 peak of Ti^{3+}.[39] The presence of Ti^{3+} is due to the oxygen deficiency in the TiO_2 lattice.[41] In general, Ti^{3+} on the TiO_2 surface plays an important role in the photocatalytic activity by trapping the photo-generated electrons, leading to unpaired charges, which promote the photoactivity. Therefore, an increase in the Ti^{3+} density facilitates effective segregation of the electrons and cavities, as well as interface charge transfer, while decreasing the probability of the occurrence of a compounding cavity, thereby increasing the photocatalytic performance. Deconvolution of the O 1 s XPS spectrum shown in Fig. 2(c) reveals two Gaussian curves centred at 530.4 and 532.2 eV, respectively. The curve centred at 530.4 eV is assigned to the Ti-O bond, while that centred at 532.2 eV is assigned to the hydroxyl groups.[42,43] The C 1 s core level spectrum shown in Fig. 2(d) consists of two peaks located at 284.8 and 286.5 eV, which are assigned to adventitious elemental carbon and C–O, respectively.[44,45]

Removal performance

Effect of material composition

To determine the effect of the material composition on ST removal performance, various amounts of biomass were used with respect to a fixed amount of TiO_2, viz. 1, 1.5, 2, and 2.5 g, with the corresponding synthesised composites referred to as TBC-1, TBC-1.5, TBC-2, and TBC-2.5, respectively. As shown in Fig. 3, a significant increase in the ST removal capacity is observed with an increase in the biomass from 1.0 to 2.0 g, under UV irradiation for 2 h at 298 K.

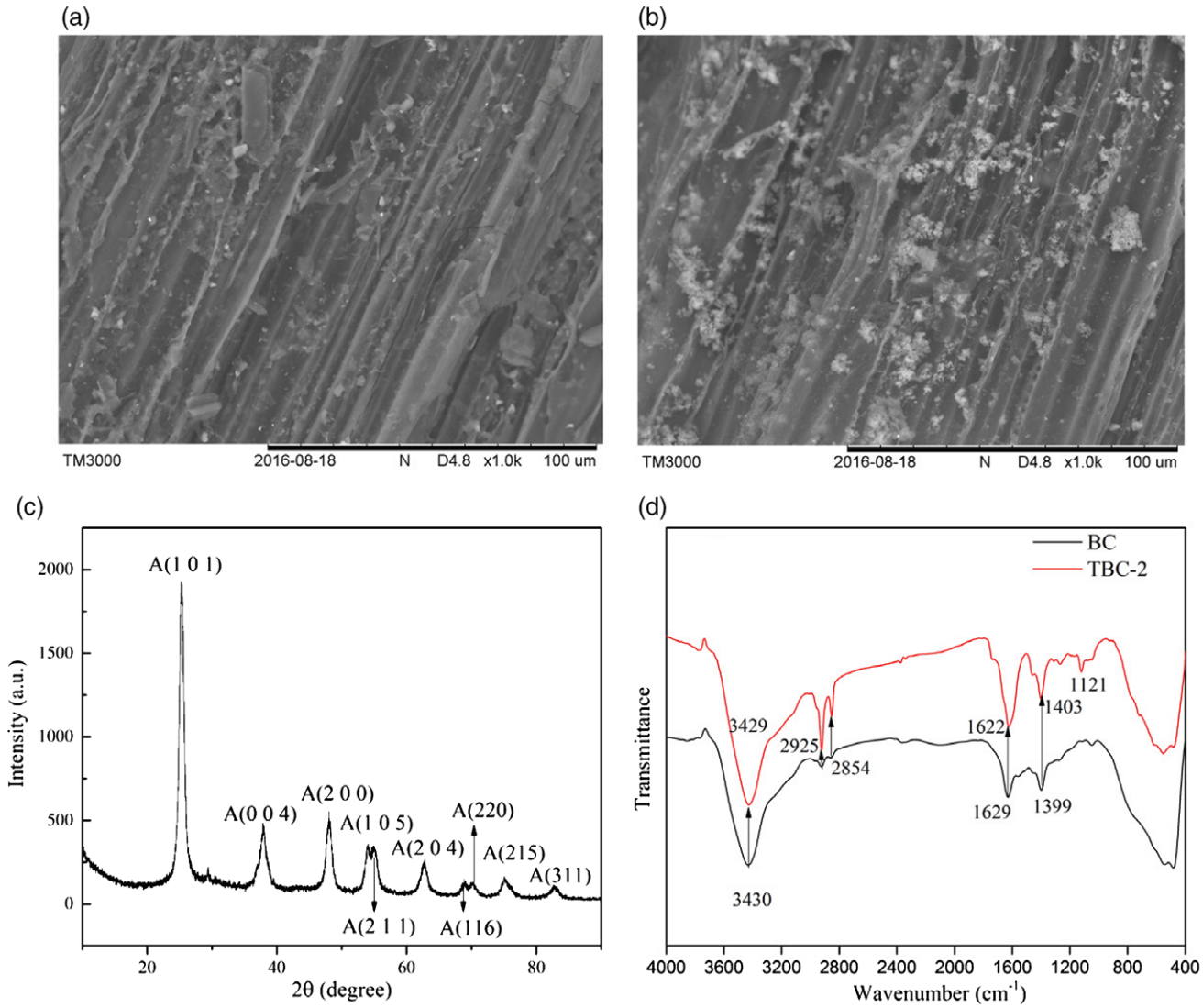

Figure 1. Characterisation of the TBC-2 composite: (a, b) SEM images, (c) XRD pattern, and (d) FTIR spectra of pristine BC and TBC-2 (arrows indicate the peak shifts).

However, the photodegradation capacity decreases substantially when the amount of biomass exceeds 2.0 g, indicating that this is the optimal biomass content. The ST removal abilities of TBC-1, TBC-1.5, TBC-2, and TBC-2.5 are 1.7, 2.3, 7.2, and 2.3 times that of the raw biochar. The ST removal capacity decreases when more than 2 g of the biomass is employed because excess BC wraps around the TiO_2, blocking the UV irradiation,[34] and thus reducing the generation and transmission of photoexcited electrons. The optimal biomass content of TBC-x was thus determined to be 2 g and was used for further investigations. Moreover, the activity of TBC-2 is much higher than that of bare BC, most likely owing to TiO_2, which increases the amount of active sites on the BC.

Effect of pH

It is noteworthy that the surface properties of the composite are determined by the synergistic effect between TiO_2 and the BC substrate. In addition, the internal condition was relatively complex owing to the various components of the BC substrate in the experimental system. This necessitated an investigation of the effect of pH on the mechanism of ST removal. This was carried out using TBC-2 and an initial ST concentration of 500 mg L^{-1}, in the pH range 3.0–11.0. The pH of the solution was adjusted by adding 0.1 mol L^{-1} NaOH or 0.1 mol L^{-1} HCl. The results shown in Fig. 4 indicate that TBC-2 remains active over a wide pH range, suggesting its insensitivity to pH changes.

Effect of the composite dosage

The material dosage is an important parameter of the removal process.[46] Sin *et al.* investigated the reaction rate of a photocatalytic oxidation process with respect to the material dosage.[47] The effect of the composite dosage on its adsorption and photocatalytic activity is possibly determined by the number of active sites and the attenuation of light absorption. Thus, it is necessary to determine the optimal amount of material required for achieving a maximum removal capacity. In this study, the influence of the composite dosage on the ST removal was investigated using different amounts of TBC-2 ranging from 0.2 to 0.6 g in steps of 0.1 g, under identical conditions, that is, 2 h of UV irradiation at 298 K. As shown in Fig. 5, a steady increase in the removal capacity is observed upon increasing the amount of the composite up to 0.4 g, beyond which the removal capacity begins to decrease. The increase in the removal capacity with increasing composite dosage within

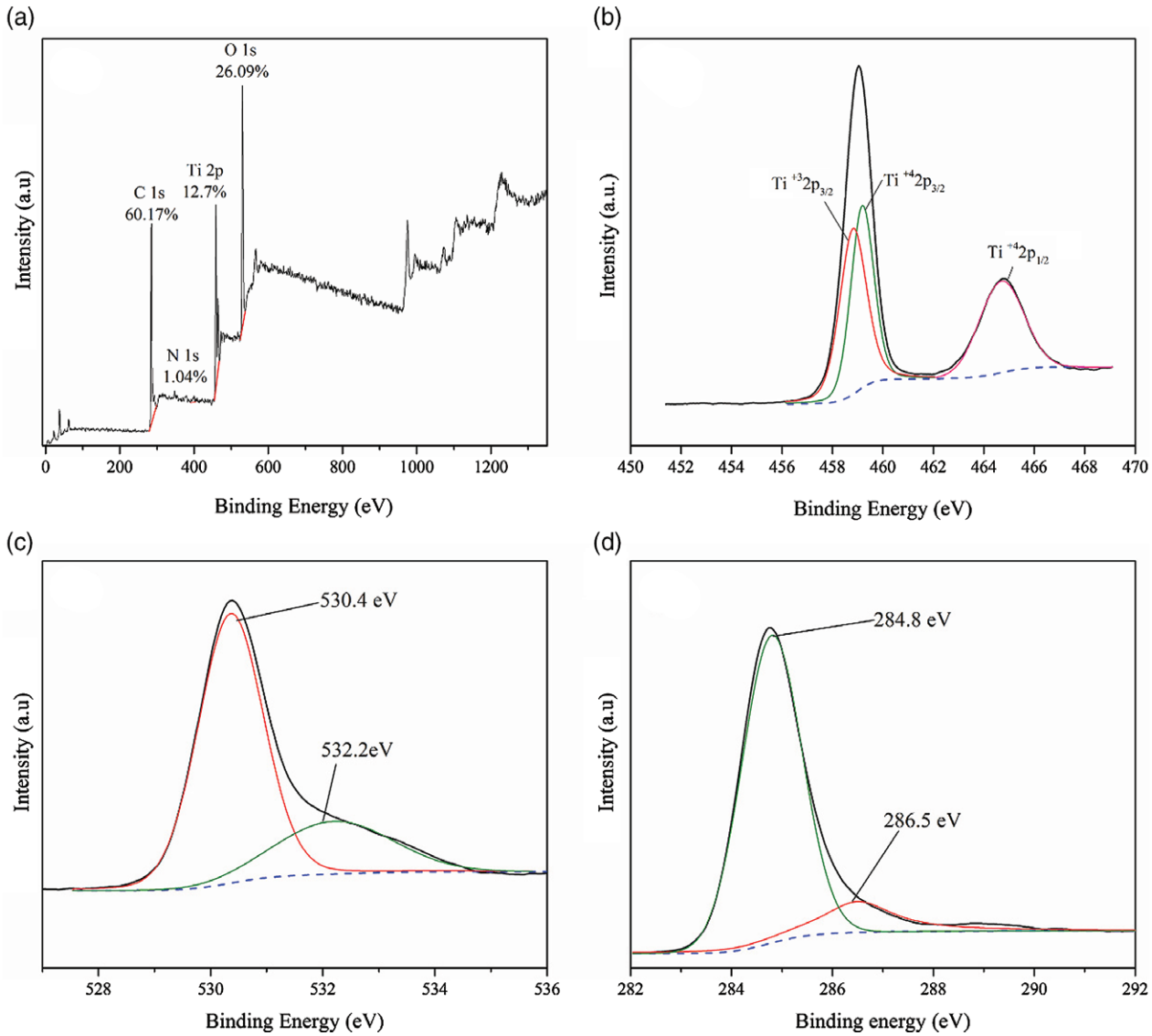

Figure 2. XPS spectra of TBC-2: (a) wide scan, (b) Ti 2p, (c) O 1 s, and (d) C 1 s.

the 0.2–0.4 g range may be attributed to: (i) an increase in the number of ST adsorption sites; and (ii) increase in the number of available active photocatalytic reaction sites on the surface of TiO_2.

In general, an increase in composite dosage increases the number of active sites on the composite surface, resulting in an increase in the amount of •OH radical. This radical is primarily responsible for the observed decolourisation of the ST solution. However, at TBC-2 concentrations higher than 0.4 g, the photodegradation capacity decreases, because: (i) the excess catalyst increases the light reflectance, thereby decreasing light penetration; (ii) the aggregation of the TiO_2 particles at high concentrations may have a screening effect that decreases the number of photosensitive surface active sites[46,48]; (iii) an increase in the recombination of the e^- or h^+ species that migrate to the surface may decrease the amounts of $\bullet O^{2-}$ and •OH; and (iv) increases in the opacity and dispersion of the TiO_2 particles at high TBC-2 concentrations may decrease the transmission of irradiation through the sample.[49] Some portions of the catalyst surface thus become unavailable for photon absorption when the TBC-2 concentration is increased, resulting in a decreased degradation rate. Based on the foregoing results, a catalyst dosage of 0.4 g was selected for subsequent investigations, from an economic perspective.

Effect of initial ST concentration

To gain insights into the effect of the initial ST concentration on the maximum ST removal capacity of TBC-2, decolourisation experiments were performed using different initial ST concentrations ranging from 50 to 700 mg L^{-1} at a pH of 8.0 and temperature of 298 K. Figure 6 shows the variation in the efficiency of the TBC-2 sample for ST removal with respect to the initial concentration of the ST. As shown, the ST removal capacity of TBC-2 increases with increase in the initial ST concentration up to 500 mg L^{-1} and then remains constant with further increase of its initial concentration due to saturation of the adsorption sites and the photodegradation capacity of TBC-2. Similar results have been previously reported for the removal of other dyes.[50] The optimum initial ST concentration of 500 mg L^{-1} for efficient ST removal was used for subsequent experiments.

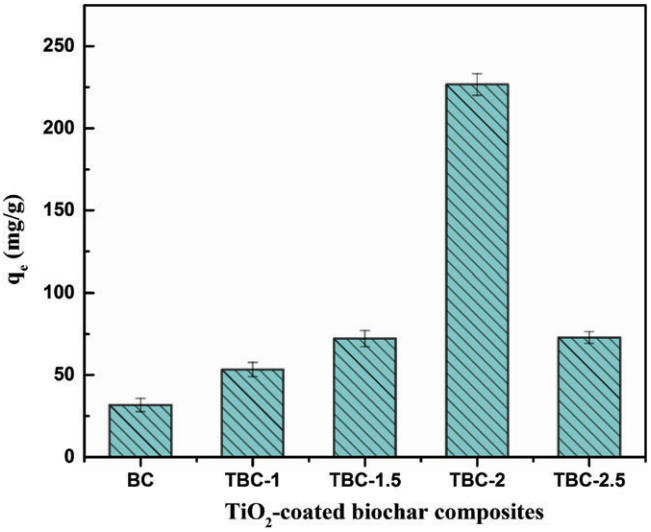

Figure 3. ST removal capacities of (a) BC, (b) TBC-1, (c) TBC-1.5, (d) TBC-2, and (e) TBC-2.5 under UV irradiation for 2 h at 298 K.

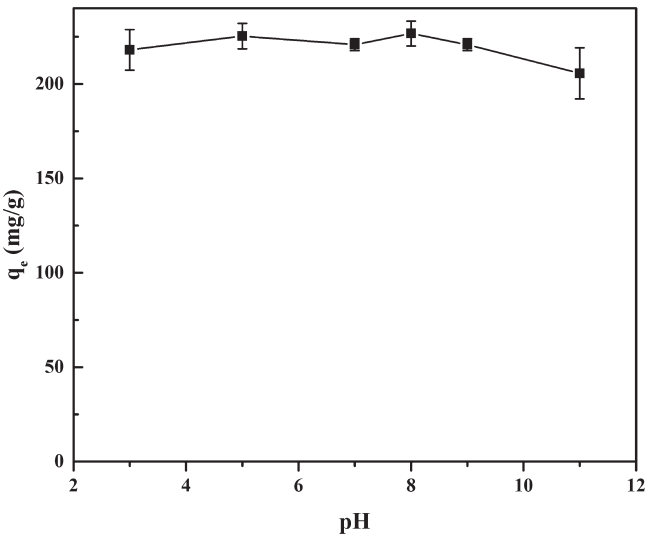

Figure 4. Effect of pH on ST removal capacity of TBC-2 under UV irradiation for 2 h at 298 K.

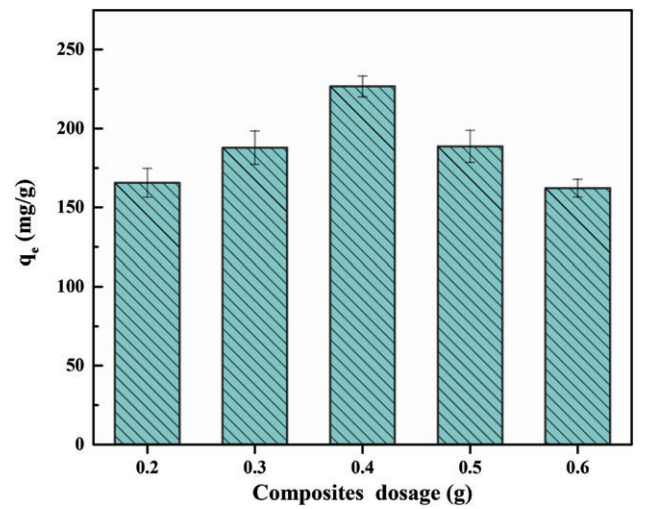

Figure 5. Effect of TBC-2 dosage on ST removal capacity under UV irradiation for 2 h at 298 K.

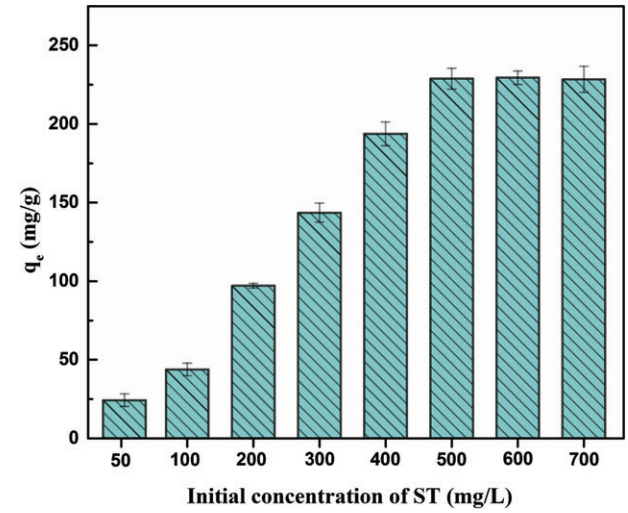

Figure 6. Effect of initial ST concentration on ST removal capacity of TBC-2 under UV radiation for 2 h at 298 K.

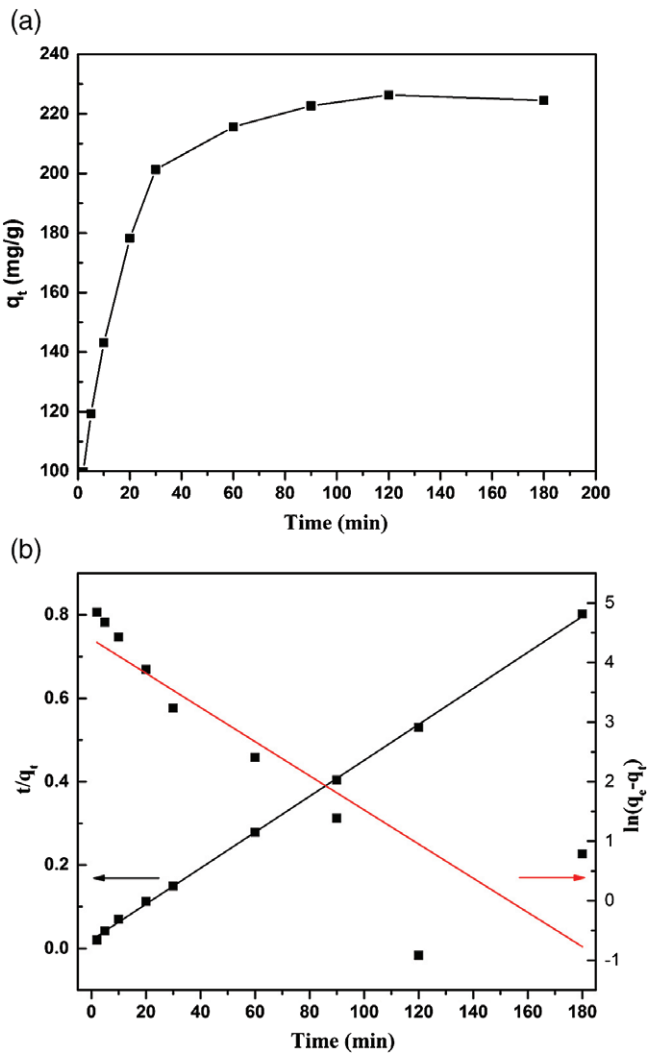

Figure 7. Kinetics of ST removal by TBC-2 under UV irradiation for 3 h at 298 K.

Table 1. Parameters of the kinetics of the ST removal process catalysed by TBC-2

	Pseudo-first-order			Pseudo-second-order		
$q_{e,exp}$	$q_{e,1}$ (mg g^{-1})	k_1 (min^{-1})	R^2	$q_{e,2}$ (mg g^{-1})	k_2 (g mg^{-1} min)	R^2
226.7	81.1	0.0287	0.755	231.9	9.421 E – 4	0.999

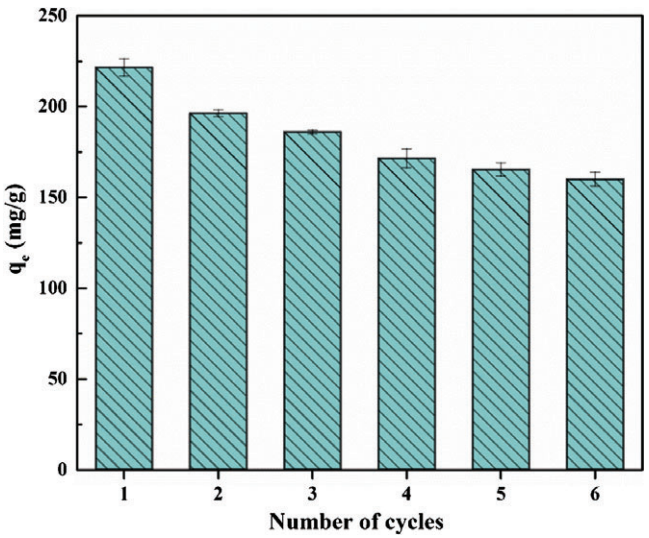

Figure 8. Reusability of TBC-2 for ST removal.

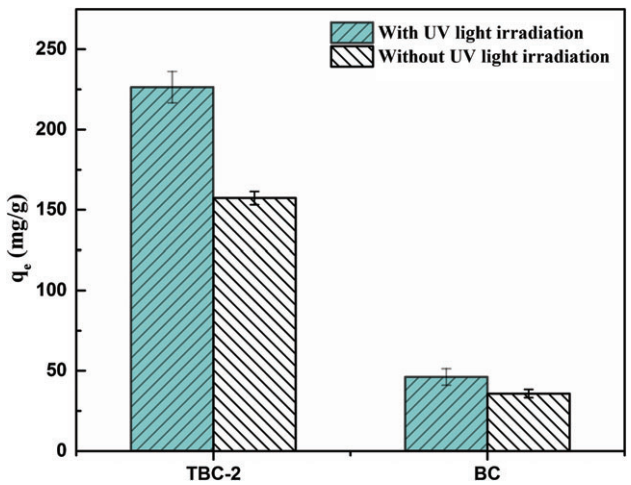

Figure 9. ST removal capacities of (a) TBC-2 and (b) BC without and with UV light irradiation for 2 h at 298 K.

Effect of the contact time

To determine the minimum contact time required for the removal of ST by TBC-2, kinetics experiments were performed using 0.4 g of the composite added to 200 mL of a 500 mg L^{-1} ST solution at a pH of 8.0. Figure 7(a) shows the ST removal capacity as a function of the contact time. Rapid removal rates are observed within the first 30 min, owing to the high number of vacant active sites on the TBC-2 surface, which facilitated interaction with ST. However, the amount of ST removed nearly saturates after 120 min, because all the active sites become occupied. The maximum removal capacity was 226.7 mg g^{-1}. The equilibrium time for ST removal is thus considered to be 120 min.

The results were further analysed using two conventional kinetic models, namely, pseudo-first-order and pseudo-second-order models.[51] Figure 7(b) shows the pseudo-first-order and pseudo-second-order kinetics of the ST removal process using TBC-2.

The pseudo-first-order model is expressed as

$$\ln\left(q_e - q_t\right) = \ln q_e - k_1 t \tag{4}$$

The pseudo-second-order model is expressed as

$$\frac{t}{q_t} = \frac{1}{k_2 q_e^2} + \frac{t}{q_e} \tag{5}$$

where q_e and q_t are the amounts of ST removed by the composite (mg g^{-1}) at equilibrium and another given time, respectively; and k_1 (min^{-1}) and k_2 (g mg^{-1} min) are the sorption rate constants of the pseudo-first-order and pseudo-second-order models, respectively. As shown in Fig. 7(b), the pseudo-second-order model produces a better fit with most of the experimental data compared with that of the pseudo-first-order model. The kinetics parameters and regression coefficients (R^2) determined by the two models are presented in Table 1. The R^2 value of the pseudo-second-order model is much higher than that of the pseudo-first-order model, indicating that the former better describes ST removal by TBC-2.

Reuse of the composite for ST removal

The reuse of a material used for decontamination is important in practical applications such as wastewater treatment.[52] We thus performed another experiment in which the TBC-2 sample was used for six recycles of ST removal. An initial ST concentration of 500 mg L^{-1}, pH of 8.0, and 120 min irradiation time was used for this experiment. After each cycle, the composite was desorbed over a period of 2 h by immersing in a solution of methanol:acetic acid = 10:1, centrifuged, and heated at 80 °C for 24 h before reuse. Figure 8 shows that the removal capacity decreases from 221.6 to 167.2 mg g^{-1} over the six cycles. This decrease is due to the detachment of TiO_2 from the support surface and following entanglement with the by-products of the photocatalytic degradation.[53] Moreover, the degradation by-products attached to the composite surface were difficult to remove, and this altered the surface properties of the composite.

Mechanism of the ST removal by TBC

To determine whether the adsorption or photocatalysis is the dominant factor for the decolourisation process, the ST removal capacity of TBC-x was evaluated without/with UV light irradiation. As shown in Fig. 9, the ST removal capacity without UV-light irradiation is 157.3 mg g^{-1}, which represents only 69.4% of the capacity (226.5 mg g^{-1}) with UV-light irradiation. This indicates that although both adsorption and photocatalytic degradation contribute to the decolourisation of ST (Fig. 9), the contribution of

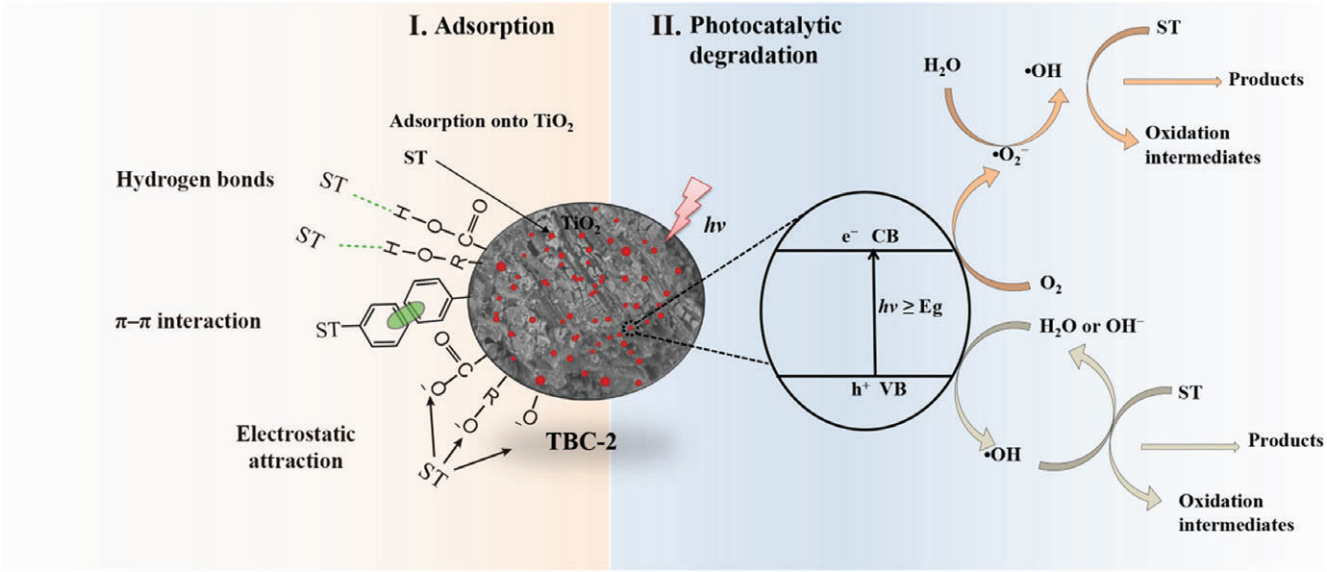

Figure 10. Schematic illustration of the adsorption and photocatalytic degradation of ST by TBC-2.

adsorption is evidently slightly higher than that of photocatalytic degradation. For comparison, the removal of ST by raw BC was also investigated with UV irradiation. In this case, there was no significant difference in the ST removal capacity compared with that without UV-light irradiation, suggesting that raw biochar had negligible photocatalytic ability, and that the TiO_2 coating was mainly responsible for the photocatalytic degradation of ST by TBC-x. In conclusion, both adsorption and photocatalytic degradation are confirmed to contribute to the decolourisation of ST (Fig. 10), with the effect of the adsorption being slightly higher than that of the photocatalysis.

Several mechanisms are involved in the adsorption process, involving interactions between the organic contaminants and the functional groups of the biochar via $\pi-\pi$ interactions, hydrogen bonding, electrostatic attraction, and hydrophobic interaction.[1,2] Furthermore, the ST adsorption capacity of TBC-2 without UV-light irradiation was much higher than that of BC, indicating that the presence of TiO_2 enhanced the adsorption capacity of BC. The coating of TiO_2 particles on BC increased the number of active sites available for the binding of ST. It has previously been reported that the coating of nanoparticles on a carbon structure increases its adsorption sites, which can be used to capture organic contaminants from water.[1]

CONCLUSIONS

TiO_2 was successfully loaded onto a biochar substrate using a modified sol–gel method. The so-produced composite exhibited very good adsorptive and photocatalytic properties and effectively removed organic pollutants from aqueous solutions. SEM and XRD investigations revealed that the material contained microcrystals and large amounts of adsorbed water and hydroxyl groups on its surface, which are beneficial for the adsorptive and photocatalytic activities of the ST removal process. Both adsorption and photocatalytic degradation contribute to the decolourisation of ST, with the effect of adsorption being slightly higher. Four types of TiO_2-coated biochar samples were investigated with respect to their ST removal efficiencies. Sample TBC-2, which was synthesised using 2 g of the processed powdered biomass, exhibited the highest decolourisation rate and ST removal capacity of 226.7 mg g^{-1}. It also exhibited good stability and activity over a wide pH range. Owing to the synergistic action between TiO_2 and biochar, TBC-2 could be a promising alternative for use in decontamination processes.

ACKNOWLEDGEMENTS

This research was financially supported by the National Natural Science Foundation of China (Grant No. 51609268 and 51521006).

REFERENCES

1 Tan XF, Liu YG, Gu YL, Xu Y, Zeng GM, Hu XJ *et al.*, Biochar-based nano-composites for the decontamination of wastewater: a review. *Bioresource Technol* **212**:318–333 (2016).
2 Tan X, Liu Y, Zeng G, Wang X, Hu X, Gu Y *et al.*, Application of biochar for the removal of pollutants from aqueous solutions. *Chemosphere* **125**: 70–85 (2015).
3 Tan XF, Liu SB, Liu YG, Gu YL, Zeng GM, Hu XJ *et al.*, Biochar as potential sustainable precursors for activated carbon production: multiple applications in environmental protection and energy storage. *Bioresource Technol* **227**:359–372 (2017).
4 Zhou Y, Gao B, Zimmerman AR, Fang J, Sun Y and Cao X, Sorption of heavy metals on chitosan-modified biochars and its biological effects. *Chem Eng J* **231**:512–518 (2013).
5 Manya JJ, Pyrolysis for biochar purposes: a review to establish current knowledge gaps and research needs. *Environ Sci Technol* **46**: 7939–7954 (2012).
6 Tan XF, Liu SB, Liu YG, Gu YL, Zeng GM, Cai XX *et al.*, One-pot synthesis of carbon supported calcined-Mg/Al layered double hydroxides for antibiotic removal by slow pyrolysis of biomass waste. *Sci Rep* **6**: (2016).
7 Yang GX and Jiang H, Amino modification of biochar for enhanced adsorption of copper ions from synthetic wastewater. *Water Res* **48**: 396–405 (2014).
8 Tan XF, Liu YG, Gu YL, Zeng GM, Wang X, Hu XJ *et al.*, Immobilization of Cd(II) in acid soil amended with different biochars with a long term of incubation. *Environ Sci Pollut R* **22**:12597–12604 (2015).
9 Zhang C, Lai C, Zeng GM, Huang DL, Yang CP, Wang Y *et al.*, Efficacy of carbonaceous nanocomposites for sorbing ionizable antibiotic sulfamethazine from aqueous solution. *Water Res* **95**:103–112 (2016).
10 Wang S, Gao B, Li Y, Mosa A, Zimmerman AR, Ma LQ *et al.*, Manganese oxide-modified biochars: preparation, characterization, and sorption of arsenate and lead. *Bioresource Technol* **181**:13–17 (2015).

11 Song Z, Lian F, Yu Z, Zhu L, Xing B and Qiu W, Synthesis and characterization of a novel MnOx-loaded biochar and its adsorption properties for Cu^{2+} in aqueous solution. *Chem Eng J* **242**:36–42 (2014).
12 Yu Z, Zhou L, Huang Y, Song Z and Qiu W, Effects of a manganese oxide-modified biochar composite on adsorption of arsenic in red soil. *J Environ Manage* **163**:155–162 (2015).
13 Wang S, Gao B, Li Y, Creamer AE and He F, Adsorptive removal of arsenate from aqueous solutions by biochar supported zero-valent iron nanocomposite: batch and continuous flow tests. *J Hazard Mater* **322**:172–181 (2017).
14 Hu X, Wang H and Liu Y, Statistical analysis of main and interaction effects on Cu(II) and Cr(VI) decontamination by nitrogen-doped magnetic graphene oxide. *Sci Rep* **6**:34378 (2016).
15 Jung K-W and Ahn K-H, Fabrication of porosity-enhanced MgO/biochar for removal of phosphate from aqueous solution: application of a novel combined electrochemical modification method. *Bioresource Technol* **200**:1029–1032 (2016).
16 Zhang M, Gao B, Varnoosfaderani S, Hebard A, Yao Y and Inyang M, Preparation and characterization of a novel magnetic biochar for arsenic removal. *Bioresource Technol* **130**:457–462 (2013).
17 Wang S, Gao B, Li Y, Mosa A, Zimmerman AR, Ma LQ *et al.*, Manganese oxide-modified biochars: preparation, characterization, and sorption of arsenate and lead. *Bioresource Technol* **181**:13–17 (2015).
18 Khanchandani S, Kumar S and Ganguli AK, Comparative study of TiO_2/CuS core/shell and composite nanostructures for efficient visible light photocatalysis. *ACS Sustain Chem Eng* **4**:1487–1499 (2016).
19 Lu Y, Yu H, Chen S, Quan X and Zhao H, Integrating plasmonic nanoparticles with TiO_2 photonic crystal for enhancement of visible-light-driven photocatalysis. *Environ Sci Technol* **46**:1724–1730 (2012).
20 Paul T, Miller PL and Strathmann TJ, Visible-light-mediated TiO2 photocatalysis of fluoroquinolone antibacterial agents. *Environ Sci Technol* **41**:4720–4727 (2007).
21 Dimitrijevic NM, Tepavcevic S, Liu Y, Rajh T, Silver SC and Tiede DM, Nanostructured TiO_2/polypyrrole for visible light photocatalysis. *J Phys Chem C* **117**:15540–15544 (2013).
22 Han F, Kambala VSR, Srinivasan M, Rajarathnam D and Naidu R, Tailored titanium dioxide photocatalysts for the degradation of organic dyes in wastewater treatment: a review. *Appl Catal A - Gen* **359**:25–40 (2009).
23 Zhang H, Chen D, Lv X, Wang Y, Chang H and Li J, Energy-efficient photodegradation of azo dyes with TiO_2 nanoparticles based on photoisomerization and alternate UV–visible light. *Environ Sci Technol* **44**:1107–1111 (2009).
24 Vinu R and Madras G, Kinetics of sonophotocatalytic degradation of anionic dyes with nano-TiO_2. *Environ Sci Technol* **43**:473–479 (2008).
25 Wang L, Liu S, Wang Z, Zhou Y, Qin Y and Wang ZL, Piezotronic effect enhanced photocatalysis in strained anisotropic ZnO/TiO_2 nanoplatelets via thermal stress. *ACS nano* **10**:2636–2643 (2016).
26 Zhou L, Liu Y, Liu S, Yin Y, Zeng G, Tan X *et al.*, Investigation of the adsorption-reduction mechanisms of hexavalent chromium by ramie biochars of different pyrolytic temperatures. *Bioresource Technol* **218**:351–359 (2016).
27 Tan XF, Liu YG, Gu YL, Liu SB, Zeng GM, Cai XX *et al.*, Biochar pyrolyzed from MgAl-layered double hydroxides pre-coated ramie biomass (*Boehmeria nivea* (L.) Gaud.): characterization and application for crystal violet removal. *J Environ Manage* **184**:85–93 (2016).
28 Liu SB, Tan XF, Liu YG, Gu YL, Zeng GM, Hu XJ *et al.*, Production of biochars from Ca impregnated ramie biomass (*Boehmeria nivea* (L.) Gaud.) and their phosphate removal potential. *RSC Adv* **6**:5871–5880 (2016).
29 Wu JC-S and Chen C-H, A visible-light response vanadium-doped titania nanocatalyst by sol–gel method. *J Photochem Photobiol A: Chem* **163**:509–515 (2004).
30 Jiang LH, Liu YG, Zeng GM, Xiao FY, Hu XJ, Hu X *et al.*, Removal of 17β-estradiol by few-layered graphene oxide nanosheets from aqueous solutions: external influence and adsorption mechanism. *Chem Eng J* **284**:93–102 (2016).
31 Liu YG, Hu XJ, Wang H, Chen AW, Liu SM, Guo YM *et al.*, Photoreduction of Cr (VI) from acidic aqueous solution using TiO_2-impregnated glutaraldehyde-crosslinked alginate beads and the effects of Fe (III) ions. *Chem Eng J* **226**:131–138 (2013).
32 Yu J, Su Y and Cheng B, Template-free fabrication and enhanced photocatalytic activity of hierarchical macro/mesoporous titania. *Adv Funct Mater* **17**:1984–1990 (2007).
33 Jiang LH, Liu YG, Liu SB, Hu XJ, Zeng GM, Hu X et al., Fabrication of β-cyclodextrin/poly (l-glutamic acid) supported magnetic graphene oxide and its adsorption behavior for 17β-estradiol. *Chem Eng J* **308**:597–605 (2017).
34 Pieróg M, Ostrowska-Czubenko J and Gierszewska-Drużyńska M, Thermal degradation of double crosslinked hydrogel chitosan mebranes. *Progr Chem Appl Chitin Deriv* **17**:67–74 (2012).
35 Li Z, Hong H, Liao L, Ackley CJ, Schulz LA, MacDonald RA *et al.*, A mechanistic study of ciprofloxacin removal by kaolinite. *Colloid Surface B* **88**:339–344 (2011).
36 Huang X, Liu Y, Liu S, Tan X, Ding Y, Zeng G *et al.*, Effective removal of Cr(vi) using β-cyclodextrin–chitosan modified biochars with adsorption/reduction bifuctional roles. *RSC Adv* **6**:94–104 (2016).
37 Sun Q, Yu HP, Zeng ZQ, Lu G and Luo YY, Surface modification of natural rubber latex film by N-Vinypyrrolidone graft copolymerization, in *Advanced Materials Research*. Trans Technical Publications 338–342 (2012).
38 Keerthana B, Madhavan J and Raj MVA, Structual and dielectric observation of Eu3+ doped titaniumdioxide nanoparticles. *Der Pharma Chemica* **6**:50–55 (2014).
39 Kim CH, Kim B-H and Yang KS, TiO_2 nanoparticles loaded on graphene/carbon composite nanofibers by electrospinning for increased photocatalysis. *Carbon* **50**:2472–2481 (2012).
40 Lassaletta G, Caballero A, Wu S, González-Elipe A and Fernández A, Photoelectron spectroscopy of metal oxide particles: size and support effects. *Vacuum* **45**:1085–1086 (1994).
41 Abidov A, Allabergenov B, Lee J, Jeon H-W, Jeong S-W and Kim S, X-ray photoelectron spectroscopy characterization of Fe doped TiO_2 photocatalyst. *Int J Mach Mach Mater* **1**:294–296 (2013).
42 Lim A and Atrens A, ESCA studies of nitrogen-containing stainless steels. *Appl Phys A - Mater* **51**:411–418 (1990).
43 Lippert T, Zimmermann F and Wokaun A, Surface analysis of excimer-laser-treated polyethylene-terephthalate by surface-enhanced Raman scattering and x-ray photoelectron spectroscopy. *Appl Spectmsc* **47**:1931–1942 (1993).
44 Ren WJ, Ai ZH, Jia FL, Zhang LZ, Fan XX and Zou ZG, Low temperature preparation and visible light photocatalytic activity of mesoporous carbon-doped crystalline TiO_2. *Appl Catal B - Environ* **69**:138–144 (2007).
45 Thierry B, Ng J, Krieg T and Griesser HJ, A robust procedure for the functionalization of gold nanorods and noble metal nanoparticles. *Chem Commun*: 1724–1726 (2009).
46 Tzikalos N, Belessi V and Lambropoulou D, Photocatalytic degradation of Reactive Red 195 using anatase/brookite TiO_2 mesoporous nanoparticles: optimization using response surface methodology (RSM) and kinetics studies. *Environ Sci Pollut R* **20**:2305–2320 (2013).
47 Sin J-C, Lam S-M and Mohamed AR, Optimizing photocatalytic degradation of phenol by TiO_2/GAC using response surface methodology. *Korean J Chem Eng* **28**:84–92 (2011).
48 Huang ML, Xu CF, Wu ZB, Huang YF, Lin JM and Wu JH, Photocatalytic discolorization of methyl orange solution by Pt modified TiO_2 loaded on natural zeolite. *Dyes Pigments* **77**:327–334 (2008).
49 Lin S-H, Chiou C-H, Chang C-K and Juang R-S, Photocatalytic degradation of phenol on different phases of TiO_2 particles in aqueous suspensions under UV irradiation. *J Environ Manage* **92**:3098–3104 (2011).
50 Jamil TS, Ghaly MY, Fathy NA, Abd el-Halim TA and Österlund L, Enhancement of TiO_2 behavior on photocatalytic oxidation of MO dye using TiO_2/AC under visible irradiation and sunlight radiation. *Sep Purif Technol* **98**:270–279 (2012).
51 Jiang L, Liu Y, Liu S, Zeng G, Hu X, Hu X *et al.*, Adsorption of Estrogen Contaminants by Graphene Nanomaterials under Natural Organic Matter Preloading: Comparison to Carbon Nanotube, Biochar, and Activated Carbon. *Environ Sci Technol* **51**:6352–6359 (2017).
52 Baek M-H, Yoon J-W, Hong J-S and Suh J-K, Application of TiO_2-containing mesoporous spherical activated carbon in a fluidized bed photoreactor – adsorption and photocatalytic activity. *Appl Catal A - Gen* **450**:222–229 (2013).
53 Liu SX, Chen XY and Chen X, A TiO_2/AC composite photocatalyst with high activity and easy separation prepared by a hydrothermal method. *J Hazard Mater* **143**:257–263 (2007).
54 Ghaly MY, Jamil TS, El-Seesy IE, Souaya ER and Nasr RA, Treatment of highly polluted paper mill wastewater by solar photocatalytic oxidation with synthesized nano TiO_2. *Chem Eng J* **168**:446–454 (2011).
55 Le HA, Chin S and Jurng J, Photocatalytic degradation of methylene blue by a combination of TiO_2-anatase and coconut shell activated carbon. *Powder Technol* **225**:167–175 (2012).

